Groundwater for Sustainable Development 18 (2022) 100793

Contents lists available at ScienceDirect

Groundwater for Sustainable Development

journal homepage: www.elsevier.com/locate/gsd

Research paper

Development and application of bio-waste-derived adsorbents for the removal of boron from groundwater

Ayesha Y. Ahmad [a], Mohammad A. Al-Ghouti [a,*], Majeda Khraisheh [b], Nabil Zouari [a]

[a] Envrionmnetal Science Program, Department of Biological and Environmental Sciences, College of Arts and Sciences, Qatar University, P.O. Box 2713, Doha, Qatar
[b] Department of Chemical Engineering, College of Engineering, Qatar University, P.O. Box 2713, Doha, Qatar

HIGHLIGHTS

- It investigates the application of bio-waste-derived adsorbents for boron removal from groundwater.
- MDPs were an effective adsorbent for boron removal from groundwater.
- Boron adsorption showed negative ΔG^{o} values that indicate a spontaneous and favorable adsorption process.
- The mechanism for $B(OH)_4^-$ adsorption is the complexing of borate by functional groups of MDPs.

GRAPHICAL ABSTRACT

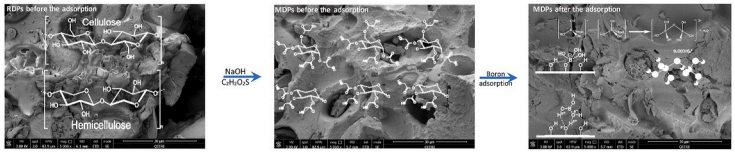

ARTICLE INFO

Keywords:
Groundwater
Treatment
Natural adsorbents
Bio-waste
Adsorption isotherms
Boron

ABSTRACT

This study investigates the development and application of bio-waste-derived adsorbents for the removal of boron from groundwater. The boron removal from groundwater was explored by bio-waste-derived adsorbents such as roasted date pits (RDPs) and modified roasted date pits (MDPs) by mercaptoacetic acid. The results were also compared with the commercially available adsorbents such as activated carbon and bentonite. Several experimental conditions, including pH, temperature, and initial concentration were investigated. Various analytical techniques were used to investigate surface characterizations, functional groups and morphological changes of the adsorbents via Fourier transform infrared spectroscopy (FTIR), Brunauer Emmett Teller (BET), and scanning electron microscopy (SEM). In addition, four adsorption models are utilized to analyze the adsorption process, including Langmuir, Dubinin-Radushkevich, Freundlich, and Temkin. The results showed that the modified roasted date pits (MDPs) could be used as an affordable, environmentally friendly, and effective adsorbent for boron removal from groundwater (GW). Negative Gibbs energy (ΔG°) values imply a spontaneous and favorable adsorption process, which is more favorable and spontaneous at high temperatures. The adsorption process was governed by positive entropy values (ΔS°), which suggests that the adsorbate–adsorbent complex may have undergone structural alterations or readjustments.

1. Introduction

Recently, Qatar has embarked on the aim of becoming the most self-sufficient and sustainable country in the Middle East. Since then, the agriculture and farming industries have flourished, allowing the country to enhance its food output. Today, groundwater (GW) is Qatar's most important renewable water resource, accounting for roughly 47.5 million m^3/year. For agricultural purposes, Qatar has traditionally

* Corresponding author.
E-mail address: mohammad.alghouti@qu.edu.qa (M.A. Al-Ghouti).

https://doi.org/10.1016/j.gsd.2022.100793
Received 26 March 2022; Received in revised form 26 April 2022; Accepted 22 May 2022
Available online 27 May 2022

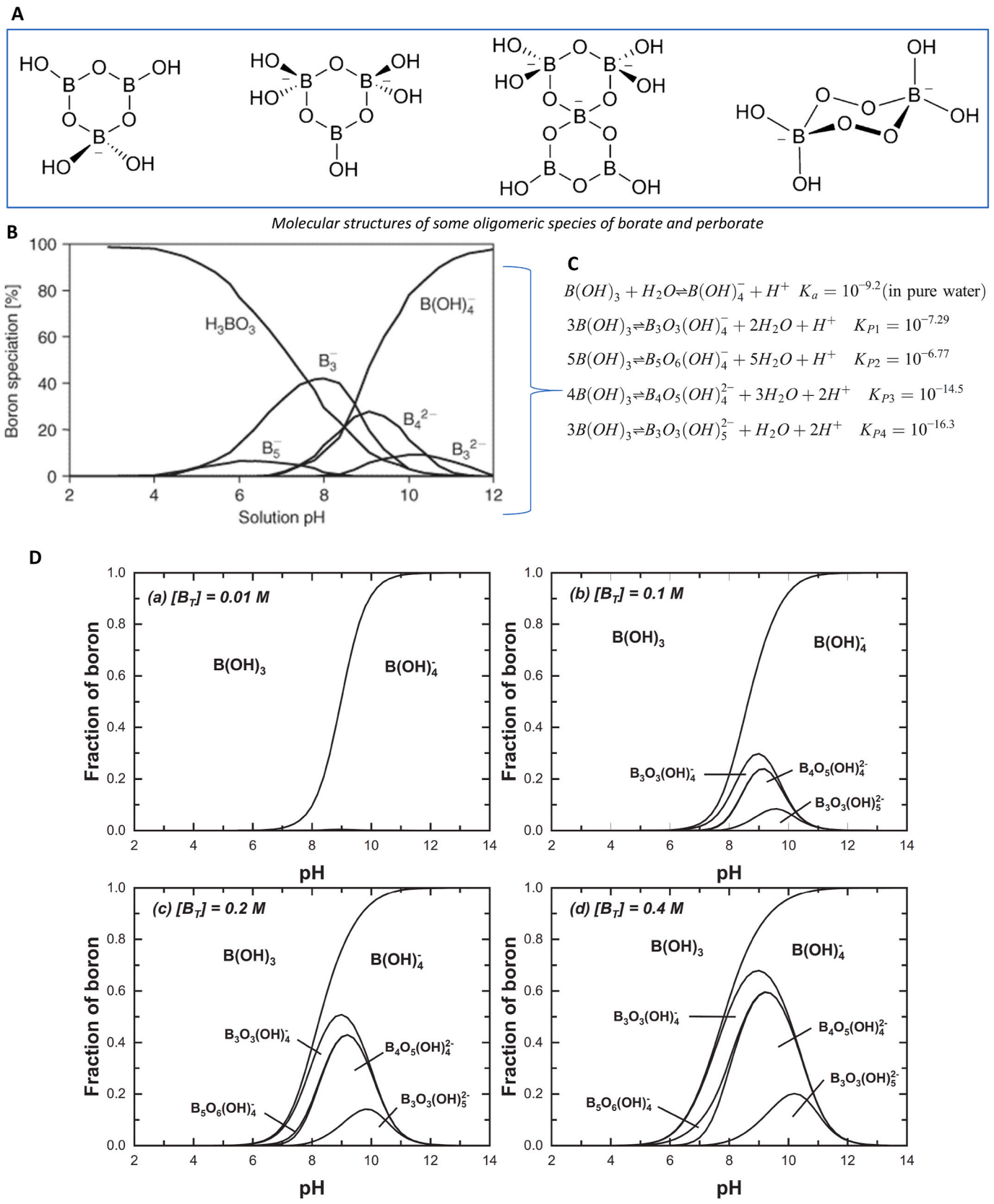

Fig. 1. **A.** Molecular structures of some oligomeric species of borate and perborate (Peters, 2014), **B.** Equilibrium boron speciation reactions (Bhagyaraj et al., 2021), **C.** Equilibrium boron speciation (Bhagyaraj et al., 2021; Jiang et al., 2014), and **D.** Speciation of borates in aqueous solution with total boron concentration varying from 0.01 to 0.4 M (Lin et al., 2021).

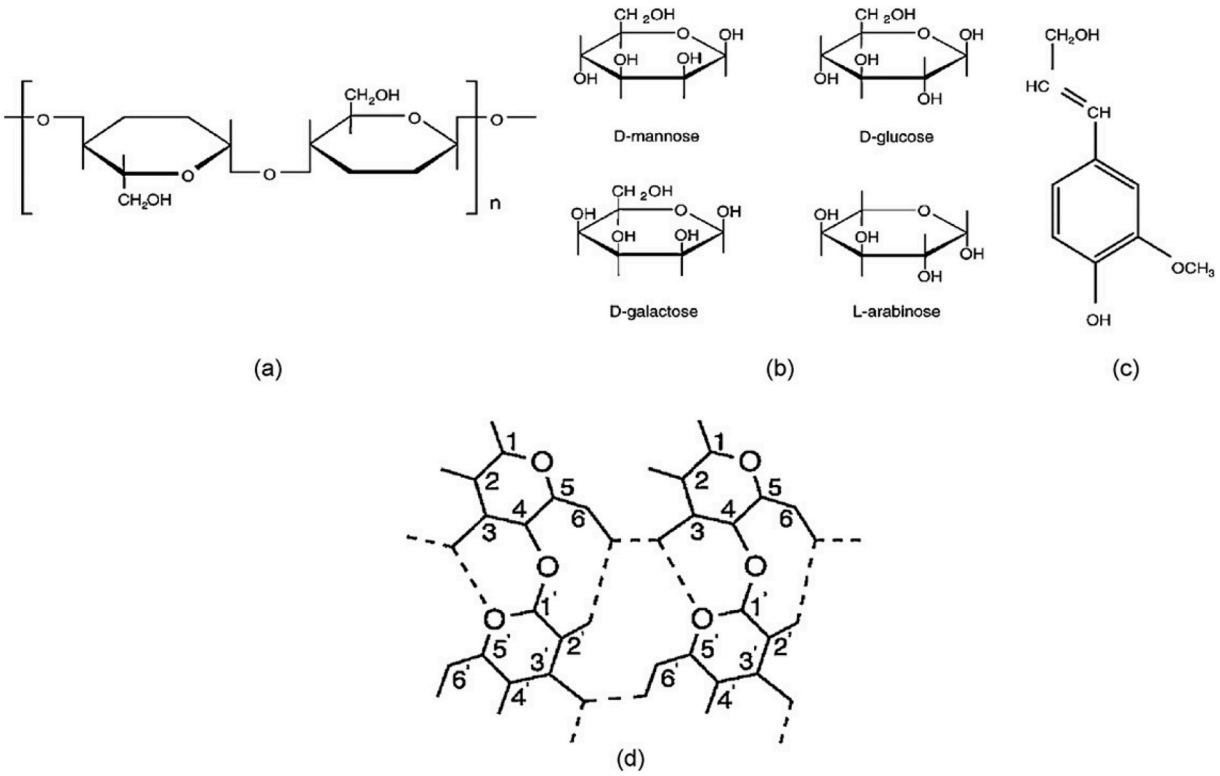

Fig. 2. (a) Cellulose molecule, (b) principal sugar residues of hemicellulose, (c) phenylpropanoid units found in lignin, and (d) hydrogen bond system of cellulose samples (El-Hendawy Abdel-Nasser, 2006; Al-Ghouti et al., 2010).

relied on GW (92 percent of total abstraction), and treated wastewater (TWW) (almost 35 percent of total production in 2015) (MDPS, Ministry of Development Planning and Statistics, 2017). The groundwater table has decreased substantially and salinity has risen as a result of 30 times more groundwater abstraction than average recharge rates (MDPS, Ministry of Development Planning and Statistics, 2018). According to previous studies, Qatari groundwater has total dissolved solids (TDS) of 1000 mg/L – 7500 mg/L, causing reverse osmosis (RO) membrane scaling and demanding costly pre-treatment procedures (Elsaid, 2017). According to our previous research (Ahmad et al., 2020), the quality of the GW has also deteriorated, with some impurities, such as metals and metalloids. Boron was found to be 1.28 mg/L. Boron is a significant source of concern since it has the potential to cause toxicity in GW. Two natural sources include weathering of igneous rocks and leaching from sedimentary boron-bearing salt deposits. Natural boron sources include rainfall with sea salt from ocean spray in coastal areas because it is highly volatile. Anthropogenic boron sources include drainage from coal mines and the mining industry, semiconductor manufacturing, agricultural use of fertilizers or pesticides, Landfill leachate, petroleum products, sewage effluents due to the use of sodium perborate in detergents and cosmetics, glass manufacturing, and fly ash (Hasenmueller and Criss, 2013). Irrigation water should not have boron in values of more than 0.5 mg/L for long-term irrigation and 1 mg/L for sensitive crops. The pKa of $B(OH)_3$ is 9.24, which can be rationalized by the relatively high electronegativity of OOH as compared to OH (Lopalco et al., 2020; Peters, 2014). Self-association of peroxoboronates takes place at higher boron concentrations between 0.025 M and 0.6 M at a neutral to alkaline pH as the predominant species, forming chair conformations with cyclic 6-membered dimers $[B_2(O_2)_n\ (OH)_{4-n}]^{2-}$. Fig. 1 shows the molecular structure of one of these dimers (Bhagyaraj et al., 2021; Peters, 2014).

Metal complexes can be formed between boron and other metals such as nickel, lead, or cadmium, which can make them more toxic (Al-Ghouti et al., 2017). Therefore, removal of boron from groundwater is highly required. Chemical remediation is used in groundwater remediation (Xie et al., 2018). Chemical remediation, on the other hand, has high operational and maintenance expenses as well as sophisticated stages; also, it produces toxic sludge (Ahmad et al., 2011). Furthermore, physicochemical GW remediation solutions such as membrane and filtration technologies, including liquid membranes, ultrafiltration membranes, polymer membranes, nanofiber membranes, electro-dialytic membranes and reverse osmosis, come in a variety of types. These various treatment techniques have their own benefits and drawbacks, which include high operation and maintenance costs, production of toxic by-products, and limited removal percentages (Temesgen et al., 2017). Biological treatment is another GW remediation technique that is being explored and developed for a variety of reasons, including cost-efficient, limited by-product production, and sustainability. However, the drawbacks of this technique are that in addition to the biosafety issues that must be addressed, the removal of pollutants from deep aquifers is not possible (Ogheneochuko et al., 2017).

To keep the system functioning, consider the operation and maintenance costs as well as the removal efficiency when researching potential treatment methods (Esmeray and Aydin, 2008; Shafiq et al., 2019). Adsorption technologies are effective in removing a variety of pollutants, are practical, straightforward, eco-friendly, not complicated, cost-effective, limited sludge production, and allow for adsorbent regeneration and recovery of metals (Dodbiba et al., 2015; Ahmad et al., 2011; Huang et al., 2016). Traditional adsorbents, such as activated carbon (AC), are costly, have environmental issues due to the non-biodegradable nature of silica gel, and have a high regeneration cost (Crini et al., 2018). However, low adsorption selectivity for boron removal is caused by AC due to low surface-active sites for boron, thus several impregnated AC is utilized for boron removal from contaminated solutions (Guan et al., 2016). The physicochemical nature of boric acid and borate showed that hydrogen bonding and hydrophobic interactions are possible adsorption mechanisms (Liu et al., 2012). The maximum adsorption capacity of boron by AC was obtained at a 5.5 pH value to be 3.5 mg/g (Köse et al., 2011). Another study found that at an initial boron

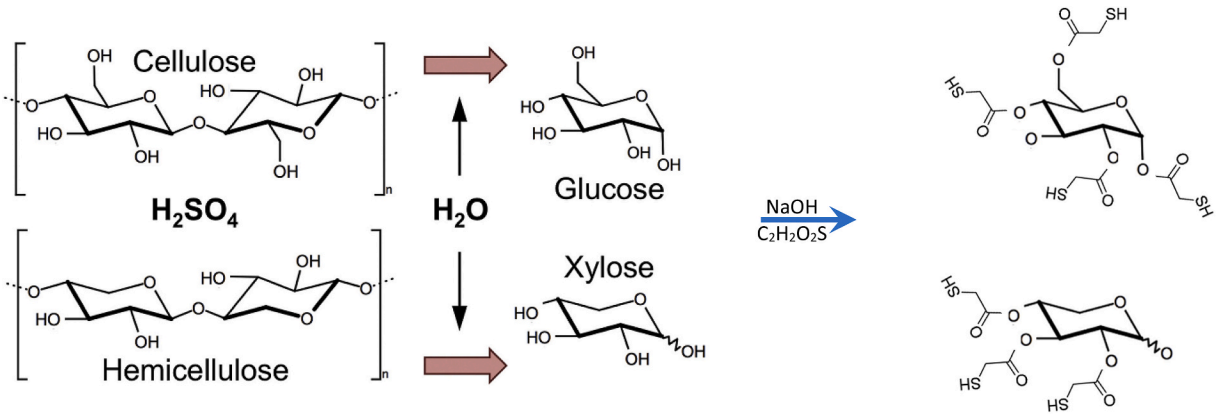

Fig. 3. Preparation of modified RDPs using mercaptoacetic acid (MAA) ($C_2H_2O_2S$) (Oyola-Rivera Oscar and Nelson, 2018; Horsfall Michael et al., 2004).

concentration of 5 mg/L the maximum percentage removal was 60% obtained at a pH value of 8–9 (Bonilla-Petriciolet et al., 2017). However, Bodzek (2015) stated that high doses of AC are required to remove 90% of boron from water.

Furthermore, bentonite clay has concerned with significant attention in metal ion pollutants treatment in aqueous solution due to its great characteristics such as the significant adsorption capacity, chemical, and mechanical stability, large specific surface area, complex porosity, lamellar structure, high cation exchange capacity, and cost-effectiveness (Zhao, 2008; Pan et al., 2011; Huang et al., 2016). The structural formula of bentonite is defined as R_x $(H_2O)_4\{(Al_{2-x},Mg_x)_2$ $[(Si,Al)_4O_{10}](OH)_2\}$ that R is the exchangeable cations of alkali and alkali-earth metals between the layers (Bananezhad et al., 2019). The study by Akpomie and Dawodu (2015) showed the potential of bentonite as a cost-efficient and environmentally friendly adsorbent that can be used to remove manganese and nickel ions from water. An increase in boron adsorption by bentonite has been noticed due to the modification on the surface of the clay with nonyl-ammonium chloride, which changes it from hydrophilic to hydrophobic (Karahan et al., 2006). Bentonite adsorption capacity toward boron was found to be 0.9 mg/g while it was 0.09 mg/g by using AC (Masindi et al., 2015). In contrast, the non-conventional adsorbents including natural materials, agricultural wastes, and industrial by-products are environment friendly, easily found, and cost-efficient (Guan et al., 2016). Various non-conventional adsorbents are utilized for water treatment, for example, eggshells for boron removal (Al-Ghouti and Khan, 2018), bentonite clay for lead removal (Al-Jlil Saad, 2015), banana peel for copper and lead removal (Vilardi et al., 2018).

Date palm waste is of great potential for adsorption metals because it is lignocellulosic fibers, which consist of cellulose, lignin, and hemicellulose with a high number of carbon atoms of low polarity and great adsorption (Ahmad et al., 2011; Shafiq et al., 2019). Lignin's functional groups bind with some metals to form coordination complexes by donating a pair of electrons (Bonilla-Petriciolet et al., 2017). Fig. 2 shows the cellulose molecules and their components. A small adsorbent dosage of date pits can remove metals and it required a short contact time for equilibrium (Shafiq et al., 2019). Date pit ash has high boron removal efficiency (71%) (Al-Ithari et al., 2011); while Al-Haddabi et al. (2015) stated the maximum removal efficiency of boron by date pit ash was 47% at neutral pH. Date pits are characterized by having oxygen functional groups (Ahmad et al., 2011). Organics' natural material sorbents were better than minerals sorbents for the boron adsorption (Liu et al., 2012). To enhance the number of active binding sites, natural sorbents require additional modifications. Date pits modifications could be achieved through physical pretreatment such as drying, grinding, and heating, it is easy, simple, and low cost; while chemical modification could be achieved by pretreatment washing with an acid such as mercaptoacetic acid, an alkali such as sodium hydroxide and potassium hydroxide; and iron salt or iron oxide mineral coating (Shafiq et al., 2019).

The equilibrium isotherm models provide parameters that describe the adsorbent – adsorbate interaction. Different adsorption models are investigated to identify the best-fitted model because no general model fits all adsorbate(s)/adsorbent processes. Adsorption models give a reliable estimation of the adsorption efficiency without using a wide range of experimental data (Al-Ghouti and Da'ana, 2020). In the current study, four adsorption models namely Langmuir, Dubinin-Radushkevich, Freundlich, and Temkin are used to describe the adsorption process. Therefore, this study aims to (i) modify roasted date pits by mercaptoacetic acid ($C_2H_2O_2S$), (ii) study the physicochemical characteristics of the prepared material, and compare them with the commercially available bentonite and activated carbon (AC) through Fourier transform infrared (FTIR) spectroscopy, Brunauer Emmett Teller (BET) analysis, and scanning electron microscopy (SEM) (iii), and explore the adsorption isotherms, adsorption mechanisms, and routes of the newly developed adsorbent for boron adsorption from groundwater.

2. Methodology

2.1. Adsorbent collection and preparation

Commercial bentonite and AC are bought from the local market. The RDPs adsorbent is prepared from the locally Qatari date (*Phoenix dactylifera* L.). Date pits are washed with distilled water and dried for 2 h in an oven at 65 °C. Then, it was roasted at 130 °C for 3 h. After that, it is ground, then rinsed continuously with deionized water. After that, the samples are dried overnight at 100 °C. The dried date grains are ground to obtain the desired size of about 0.25 mm–0.125 mm. Next, the samples were sieved; then the samples were preserved in sterilized containers.

2.2. Preparation of modified RDPs

Fig. 3 illustrates the preparation of the modified RDPs. Firstly, the roasted date pits powder (about 50 g) was soaked with H_2SO_4 (100 mL, 98% w/w) for half an hour and kept overnight (Yadav et al., 2013). Then it is washed with distilled water, centrifuged, and dried. NaOH solution (200 mL, 1 M) was added to resulted date pits with continuous mixing for 60 min. Then mercaptoacetic acid (MAA) ($C_2H_2O_2S$) (1 M) also known as Thioglycolic acid (TGA) was added with continuous mixing for 3 h to convert hydroxyl groups to mercapto groups also known as a thiol group or a sulfhydryl group (-SH) and then allowed to stand for overnight. Then the product was filtered, washed, centrifuged, and dried at 100°C overnight.

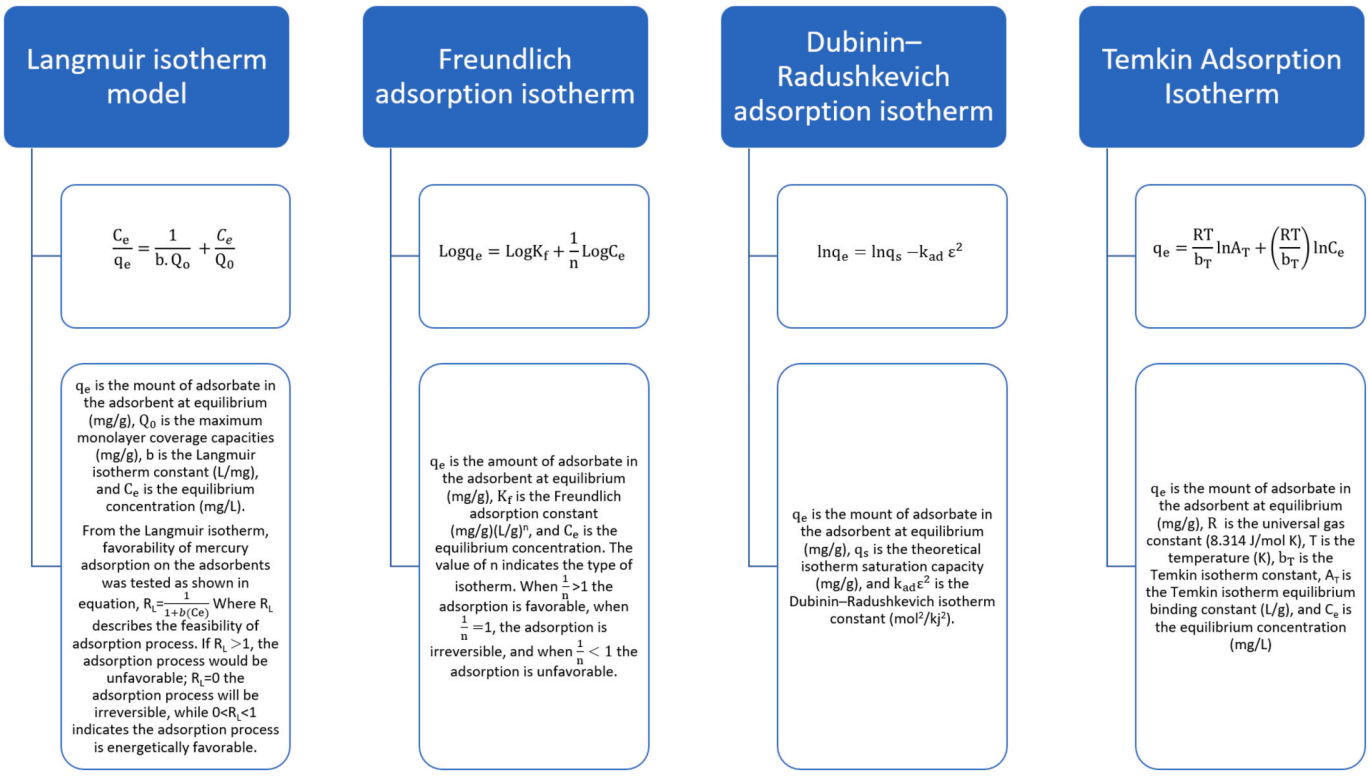

Fig. 4. The used adsorption isotherm model.

2.3. Characterization of the adsorbents

The morphological characteristics of the prepared adsorbents were determined using SEM, while the functional groups present on the surface of the adsorbents were investigated using FTIR (FT-IR/FT-NIR Spectrometer- Spectrum 400). FTIR analysis is conducted using PerkinElmer 400 spectrum instrument universal attenuated total reflectance (UATR). The absorbance spectra are obtained in the 4000 cm^{-1} - 400 cm^{-1} range. The surface area and pore size distribution of the adsorbents were determined using BET (model Aim Sizer-AM301).

2.4. Batch adsorption experiments of boron

Various factors were investigated including pH (2, 4, 6, 8, and 10), initial concentration (5, 10, 15, 20, 30, 40, 50, 60, 80, and 100 mg/L) and temperature (25, 35, and 45 °C). A 0.05 g of the adsorbent (roasted date pits (RDPs), modified roasted date pits (MDPs), bentonite, activated carbon (AC)) was added to 50 mL boric acid of various concentrations and then were shaken at 165 rpm for 24 h which we consider it as the equilibrium time, at a temperature-controlled shaker. After that, inductively coupled plasma mass spectrometry (ICP-MS) was used to determine the concentration of boron after filtering the samples. The boric acid stock solution of 100 mg/L was prepared by adding 0.572 g of boric acid into 1 L distilled water and then different dilutions (5, 10, 15, 20, 30, 40, 50, 60, 80, and 100 mg/L) were prepared. The pH was adjusted by using HCl (0.05 M) for acidic pH values and NaOH (0.05 M) for basic pH values.

2.5. Adsorption isotherms

Modeling adsorption isotherm involves data from batch adsorption experiments such as a series of equilibrium concentrations with respect to the resulting adsorption efficiency. The adsorption capacities (q_e) and percentage of removal (%) are calculated by equations (1) and (2), respectively (Al-Ghouti and Da'ana, 2020).

$$qe = \frac{(Ci - Ce) \times V}{m} \quad (1)$$

$$\text{Percentage Removal } (\%) = \frac{C_i - C_e}{C_i} \times 100 \quad (2)$$

Where C_i is initial concentration (mg/L) and C_e is equilibrium concentration (mg/L), m is the adsorbent's mass (g) and V is the solution's volume (L).

In the current study, four adsorption isotherms were used to describe the adsorption process, namely Langmuir isotherm model, Freundlich isotherm model, Dubinin-Radushkevich isotherm model, and Temkin isotherm model. Fig. 4 illustrates the linear equation, constants, and adsorption parameters of the studied isotherm models.

2.6. Thermodynamic studies

The determination of the thermodynamic parameters is critical for understanding the adsorption process because they help in determining whether the adsorption is favorable, spontaneous, endothermic, or exothermic (Al-Ghouti and Da'ana, 2020). The negative of ΔG° indicates that the adsorption is spontaneous. However, if ΔH° is a positive value, then the reaction is endothermic and if ΔH° is negative, then it is an exothermic reaction. The positive ΔS° value indicates the adsorbent's affinity towards the adsorbate. The adsorption thermodynamic parameters could be given from equations (3)–(5), then the values of ΔH° and ΔS° could be found by Van't Hoff plot of ln (K_e) versus (1/T) (Al-Ghouti and Da'ana, 2020).

$$\Delta G^\circ = - RT \ln K_a \quad (3)$$

$$\Delta G^\circ = \Delta H^\circ - T\Delta S^\circ \quad (4)$$

$$\ln K_a = -\frac{\Delta H^\circ}{RT} + \frac{\Delta S^\circ}{R} \quad (5)$$

Table 1
Crystal radius, hydrolysis constant, and electronegativity of boron.

Characteristics	Value	References
Crystal radius r_{cryst} (Å)	2.44	Shannon (1976); Corti and Crovetto (1980)
Hydration radius r_s (Å)	2.61	Wang and Ira, 2012; Yizhak (1989)
Hydrolysis constant pKa	Boric acid $B(OH)_3$ 9.24 (Weakly acidic cation)	Miessler et al. (2014); Wulfsberg (1995); Nagul et al. (2015)
Pauling electronegativity	2.051	Harris, 2011 and Harris, 2011

Table 2
Brunauer Emmett Teller (BET) surface area parameters for different adsorbents.

Parameters	Activated Carbon	Bentonite	Roasted Date Pits	Modified Roasted Date Pits
Surface Area (m^2/g)	179	34.7	28.4	29.7
Single Point Total Pore Volume (cm^3/g)	0.165	0.187	0.0837	0.0980
Single Point Adsorption Microporous Volume (cm^3/g)	0.0780	0.0146	0.0100	0.0140
Single Point Average Pore Rdius (nm)	1.88	10.8	5.7	6.31

Where the gas constant (8.314 J/mol.K) is denoted as R, the temperature in Kelvin (K) is denoted as T, and the equilibrium thermodynamic constant is denoted as K_a which could be calculated from equation (6).

$$K_a = \frac{q_e}{C_e} \tag{6}$$

Thus, it is reasonable to use the Langmuir isotherm constant to estimate the unitless value of K_a (Bonilla-Petriciolet et al., 2017).

2.7. Statistical analysis

Analysis of variance was used to statistically test the results of the adsorption experiment because the experimental designs are completely randomized design (CRD). ANOVA for two factors using Microsoft Excel 2016 is utilized to investigate the link between temperature and initial boron content. Because the experiment was a single factor experiment, ANOVA for a single factor was utilized to investigate the pH effect on boron adsorption capacity. In addition, the Chi-squared test (χ^2) and the coefficient of determination (R^2) is used to investigate the best-fit adsorption isotherm model.

3. Results and discussion

3.1. Physical and chemical characteristics of adsorbates

Metal ions with higher electronegativity have the ability to adsorb easier than metals with lower electronegativity, and metals with higher hydrolysis constants improve the capacity of adsorption, whereas bigger ionic radius metals' have lower density charge and weaker electrostatic attraction, leading to the reduction in the adsorptive capacity (Minceva et al., 2008). To find a possible attractive site between boron and adsorbents, characteristic properties such as crystal radius and equilibrium constants for adsorbate ions are shown in Table 1. Moreover, it is essential to study the physicochemical properties of adsorbents to better understand the adsorption process and have insight into the governing mechanisms of adsorption.

3.2. Brunauer Emmett Teller (BET) analysis

Surface area parameters for different adsorbents were conducted using BET using nitrogen physisorption as shown in Table 2 below. The

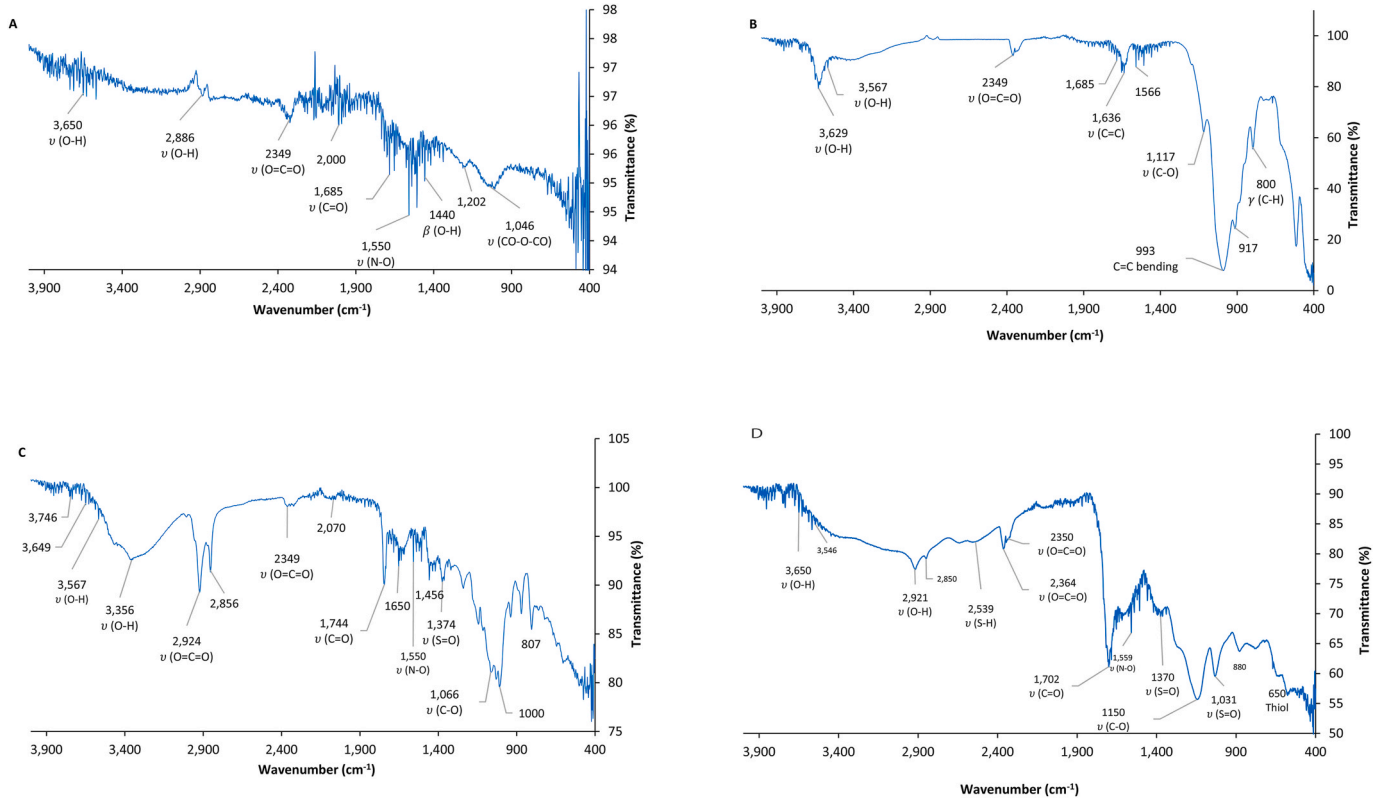

Fig. 5. FTIR Spectra for (A) activated carbon, (B) bentonite, (C) RDPs, and (D) MDPs.

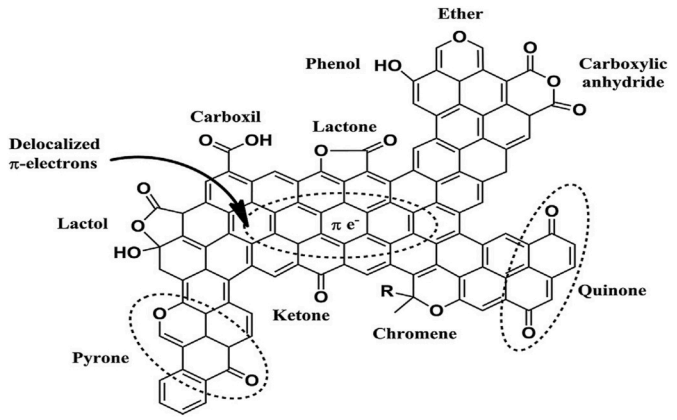

Fig. 6. Surface oxygenated groups presented in activated carbon (Velo-Gala et al., 2014).

order of surface area for the adsorbent is shown as AC > bentonite > MDPs > RDPs. AC shows the highest surface area of 178.79 m^2/g while RDPs show the lowest surface area of 2.84 m^2/g, while bentonite and MDPs were 34.7 and 29.7 m^2/g, respectively. The pore volume for different adsorbents is ordered as bentonite > AC > RDPs > MDPs. AC shows the highest pore volume (0.187 cm^3/g), while RDPs show the lowest pore volume (0.0837 cm^3/g), while bentonite and MDPs were 0.187 and 0.0980 cm^3/g, respectively. The adsorption microporous volume follows the order AC > bentonite > RDPs > MDPs, in which AC has the highest microporous volume (0.078 cm^3/g), while RDPs show the lowest microporous volume (0.0100 cm^3/g), while bentonite and MDPs were 0.0146 cm^3/g and 0.0140 cm^3/g, respectively. The order of average pore radius for different adsorbents is as bentonite > MDPs > RDPs > AC. Bentonite has mesopores diameters which is the highest average pore radius (10.81 nm), MDPs and RDPs have mesopores diameters of 5.7 nm and 6.31 nm, respectively, while AC shows micropores diameters such that the average pore radius is the lowest (1.88 nm). Comparative results to the current results are shown by other studies. Al-Ghouti et al. (2017) stated that the RDPs had a total surface area of 99.76 m^2/g and cumulative pore volume of 0.14 cm^3/g, while Alhamed (2009) stated that RDPs had a total surface area of 1.2 m^2/g and cumulative pore volume of 0.23 cm^3/g. While the total surface area for AC was 359 m^2/g in the study of Djilani et al. (2015). Besides, the study of Andrade et al. (2018) showed that the total surface area and cumulative pore volume of bentonite were 28 m^2/g.

3.3. Fourier transform infrared spectroscopy (FTIR) analysis

Fig. 5 shows the peaks that are approximately assigned for different functional groups for AC, bentonite, RDPs, and MDPs. The identification of the functional group from the absorbance spectra is adopted from the study by Socrates (2015) and Smith and Dent (2019), where υ is stretching, β is in-plane bending and γ is out-of-plane bending. Fig. 5A shows that AC is characterized by different hydroxyl groups such as β (OH) at 1440 cm^{-1} and υ (OH) at 2887 cm^{-1} and 3650 cm^{-1}, in addition to oxygenated groups such as at 2349 cm^{-1} 1205 cm^{-1}. Furthermore, Fig. 6 illustrates the oxygenated groups on the surface of AC. Bentonite is characterized by hydroxyl groups like υ (OH) at 3629 cm^{-1} and 3567 cm^{-1}, in addition to oxygenated groups such as at 2349 cm^{-1} and 1117 cm^{-1} as shown in Fig. 5B. Moreover, Fig. 7 represents the silanol and aluminol functional groups and their protonation and deprotonation states on the edge of bentonite (Bananezhad et al., 2019; Strawn, 2021).

Moreover, RDPs are characterized by hydroxyl groups such as υ (OH) at 3356 cm^{-1} and 3567 cm^{-1}, in addition to oxygenated groups such as at 1374 cm^{-1} and 1744 cm^{-1} as shown in Fig. 5C. Fig. 5D shows that the modification of date pits has different new functional groups. The MDPs have oxygen groups, mainly carbonyl, alcohol, and aromatic groups such as at 1370 cm^{-1} which is assigned to (S═O), and at 1703 cm^{-1} which is assigned to stretching vibrations of υ (C═O) ester groups, suggesting that mercapto-acetate functions with thiol groups are presented. Moreover, the peak at 650 cm^{-1} implied the weak absorbance of υ (S–H) groups, which represent the thiol group in addition to S–H bond stretching appearing at 2539 cm^{-1}. A similar finding of adding sulfur functional group at peaks 613 cm^{-1}, 1014 cm^{-1}, and 1075 cm^{-1} after date pits modification is found by Al-Ghouti et al. (2019). As shown in Fig. 5D, thiol groups were introduced into the adsorbent date pits, in addition to hydroxyl groups such as υ (OH) at 2921 cm^{-1} and 3650 cm^{-1}. The adsorption process is significantly enhanced due to the presence of these functional groups on the adsorbent surface. The results of the available functional groups on the surface of the date pits such as alcohol O–H, aldehyde, ketone, ester C═O, and alcohol, ester C–O are compared with the reported study by Al-Ghouti et al., 2010); Al-Ghouti et al., 2017.

3.4. Scanning electron microscopy (SEM) analysis

SEM is a significant analytical technique that is extensively utilized to analyze the adsorbent surface morphology. Fig. 8 shows SEM images that demonstrate the morphology, pore structure, and homogeneity of AC, bentonite, RDPs, and MDPs before and after boron adsorption. Due to the preparation procedure and mechanical grinding, all adsorbents

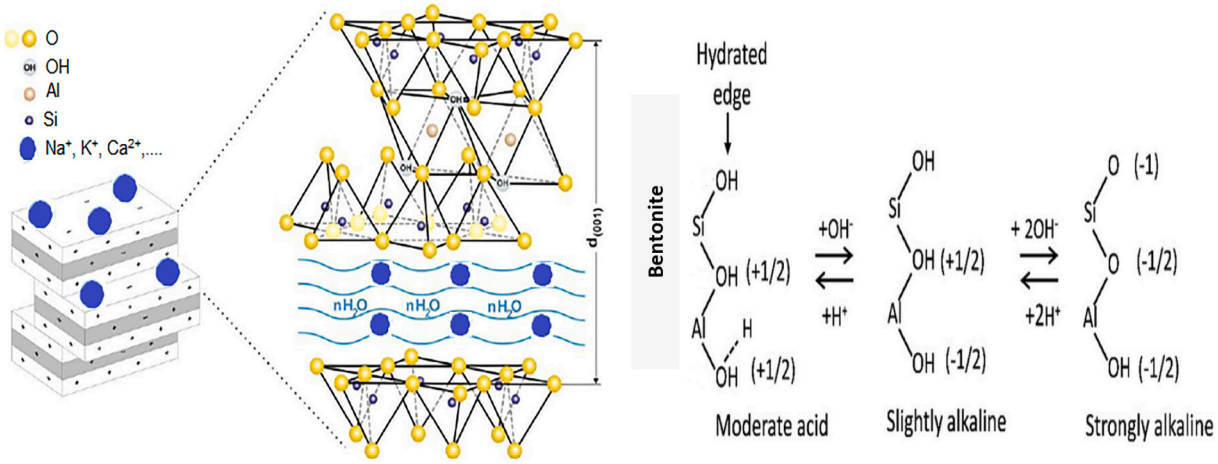

Fig. 7. Edge of bentonite mineral showing the silanol, aluminol functional groups, and their protonation and deprotonation states (Bananezhad et al., 2019; Strawn, 2021).

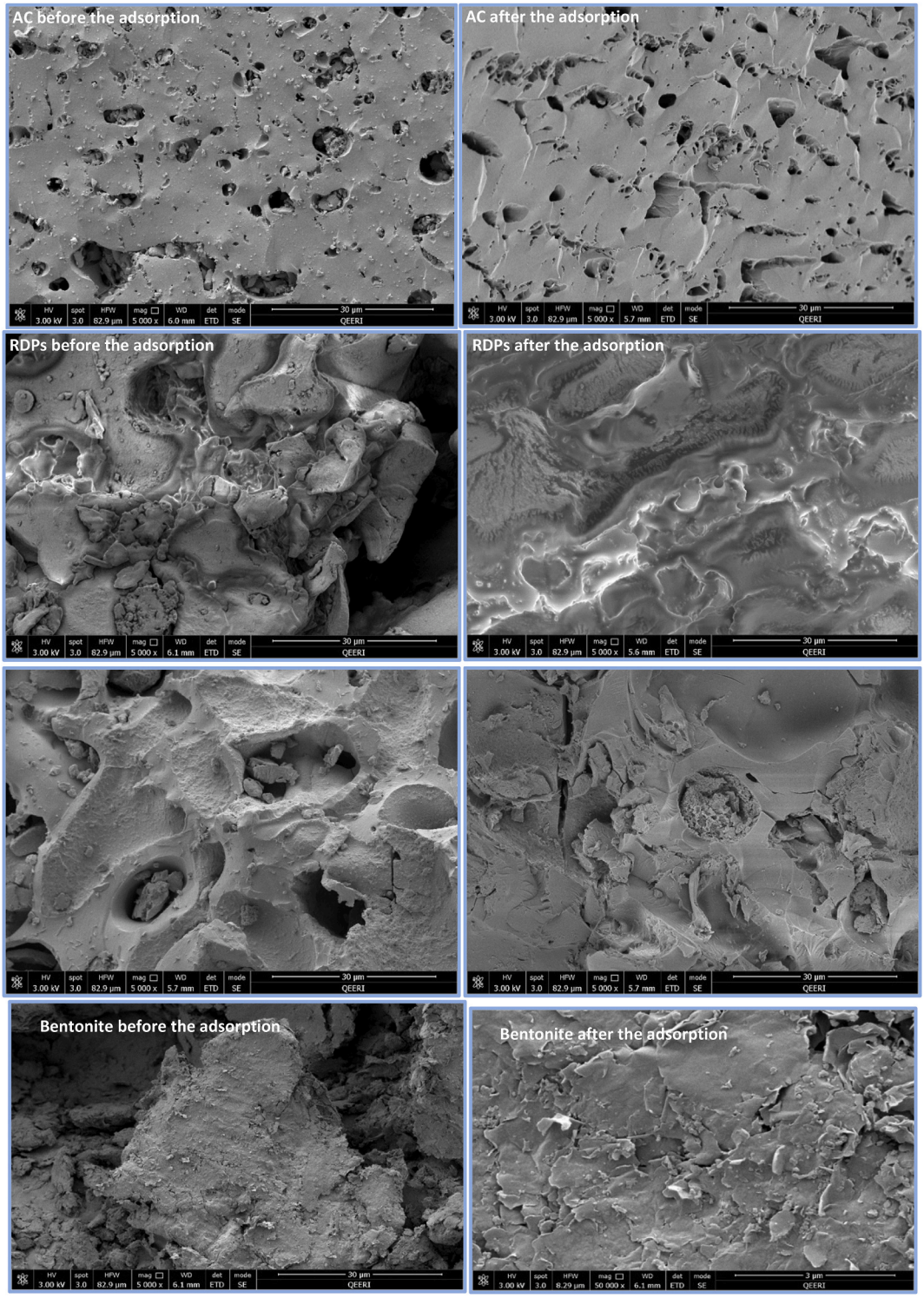

Fig. 8. Morphological characterization of AC, RDPs, MDPs, and bentonite before and after boron adsorption.

had irregular forms and sharp edges. The surface structure of bentonite was less rough and smoother than that of other adsorbents. Both adsorbents AC and MDPs have a rougher surface structure with more pores and edges than bentonite and RDPs. Thus, the chemical modification increased the adsorbent surface area that further enhancing the capacity of the adsorption process. AC and MDPs have diverse pore sizes and shapes that are narrow and confined which facilitate capturing the different adsorbates. The very tiny pores that characterized AC are mainly because of the activation process and the successive release of volatile organic species. While RDPs show larger pores with a random arrangement that facilitates the adsorption on the surface. These findings are in support of the BET surface area results. The existence of fine particles on the adsorbent's outer surface is also demonstrated. Impurities detected in the original RDPs could be due to the presence of such debris. The elimination of such organic contaminants may have been aided by heat treatment and roasting and hence, their appearance is less on MDPs surface. The morphology of the AC and RDPs particles was similar to that observed in the study by Al-Ghouti et al., 2017). It is clear

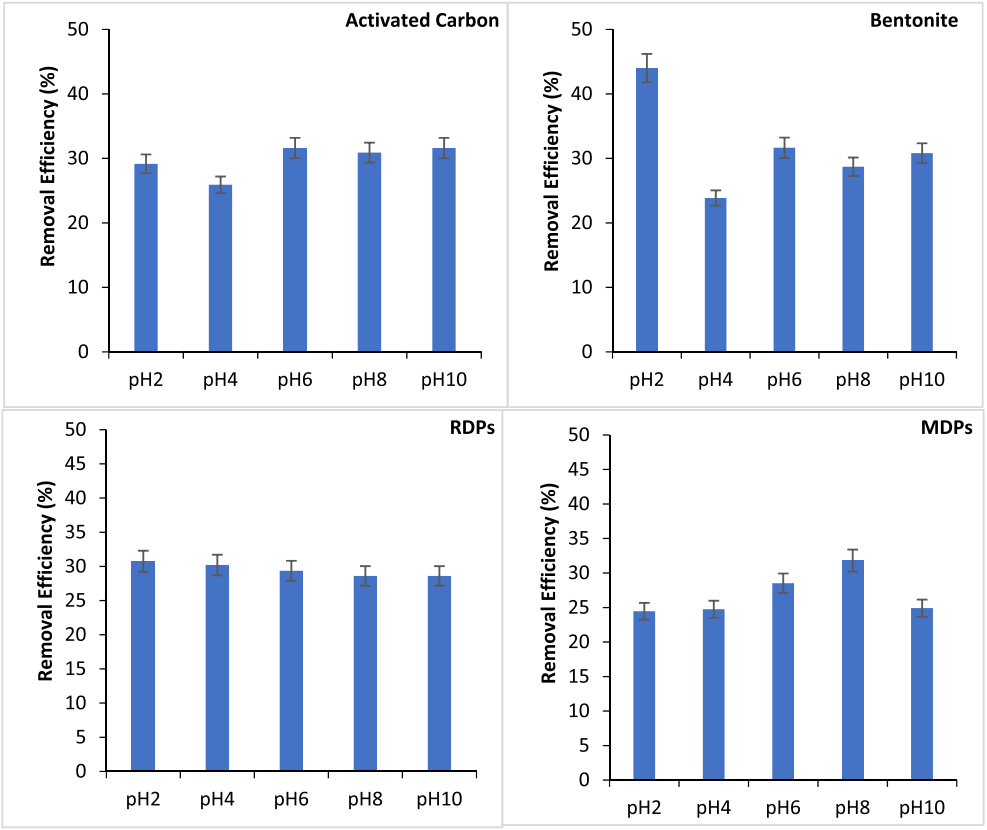

Fig. 9. Study of the influence of pH on boron adsorption using activated carbon, bentonite, RDPs, and MDPs.

from the after-adsorption images that AC and MDPs have a high number of pores that indicate a significant capacity for trapping adsorbates. The change in the adsorbent structure is also shown, as the small pores are reduced, while the large pores are increased which indicates a possibility of different adsorption mechanisms. In addition, the structure is smoothed for AC, RDPs, and MDPs after the adsorption process compared with the relatively rough and irregular surfaces before the adsorption. The rough and irregular surfaces indicated a higher adsorption capacity by trapping the adsorbate.

3.5. Effect of pH

The adsorption of metal ions from aqueous solutions is highly dependent on the solution pH as it determines the hydrogen and hydroxyl ion concentrations (Al-Ghouti et al., 2017). Fig. 9 shows boron adsorption efficiency under different pH values. The boron adsorption efficiency was about 31.65% for bentonite at pH 6, about 31.6% for AC at pH 6, and about 31.8% for MDPs at pH8, 30.75%, and 29.35% at pH 2 and pH 6, respectively for RDPs. Fig. 10A illustrates an example of the reaction of boron adsorption onto bentonite.

Moreover, since boron adsorption is affected by pH conditions, which can alter adsorbent surface properties and the dominant boron species accessible in the aqueous solution, the result suggests that a weak acid solution (pH 6) was effective for boron adsorption. Fig. 10B shows different pathways for the dissociation of boric acid. Since boric acid has a pKa value of 9.24 so $B(OH)_3$ is the dominant species at pH < 9 whereas at pH more than 9, borate $B(OH)_4^-$ is the dominant species (Al-Ghouti and Khan, 2018). Borate is negatively charged; it is electrostatically attracted with hydrogen ions, while it is electrostatically repulsed with hydroxyl ions. It is well known that changes in pH alter the degree of ionization and the surface charge of adsorbents. Hence, boron adsorbent could have different mechanisms such as ion exchange, electrostatic interactions, and other chemical bindings besides the physical adsorption. Fig. 10D represents the adsorption mechanism of boric acid onto RDPs.

As mentioned above at weak acidic conditions, AC offered a higher adsorption efficiency in comparison to RDPs and MDPs. While in a neutral environment, it only reaches around 30% removal efficiency. At a strong acidic condition (pH 2), the removal efficiency is decreased using MDPs due to the electrostatic repulsion between the boric acid $B(OH)_3$ with the protonation hydroxyl and carbonyl functional groups (Al-Ghouti et al., 2010). Additionally, the presence of chloride ions competes with boron ions on the positive adsorption sites. However, the presence of excess chloride ions at a low pH value caused a high boron removal efficiency due to Cl^- interaction with the anion functional groups on the adsorbent surface hence Cl^- attracting boric acid $B(OH)_3$. The increase of boron adsorption by AC and MDPs with increasing the pH of the solution could be due to the complexation reaction between the borate $B(OH)_4^-$ and OH^- on the adsorbent's surface. On the contrary, at higher alkalinity conditions, adsorption capacity decreased due to the competition for the active adsorption sites between the dominant species of boron (borate) $B(OH)_4^-$ and hydroxyl ions.

3.6. Influence of initial concentration

As shown in Fig. 11 the adsorption of boron is decreased when the initial concentration is 100 mg/L for all adsorbents as a result of the unavailability of vacant sites. Table 4 represents the adsorption capacity obtained by all used adsorbents for the removal of boron. Our results showed that when the initial boron concentration was 30 mg/L, the highest removal efficiency was 36% using MDPs, 50% using RDPs at 40 mg/L, 18% using AC at 10 mg/L, and 54% using bentonite at 30 mg/L. Fig. 12 illustrates the adsorption mechanism of boron by bentonite. The high adsorption capacity at low concentrations is attributed to the availability of unoccupied adsorption sites. The increased removal efficiency was obtained as a result of increasing boron concentration.

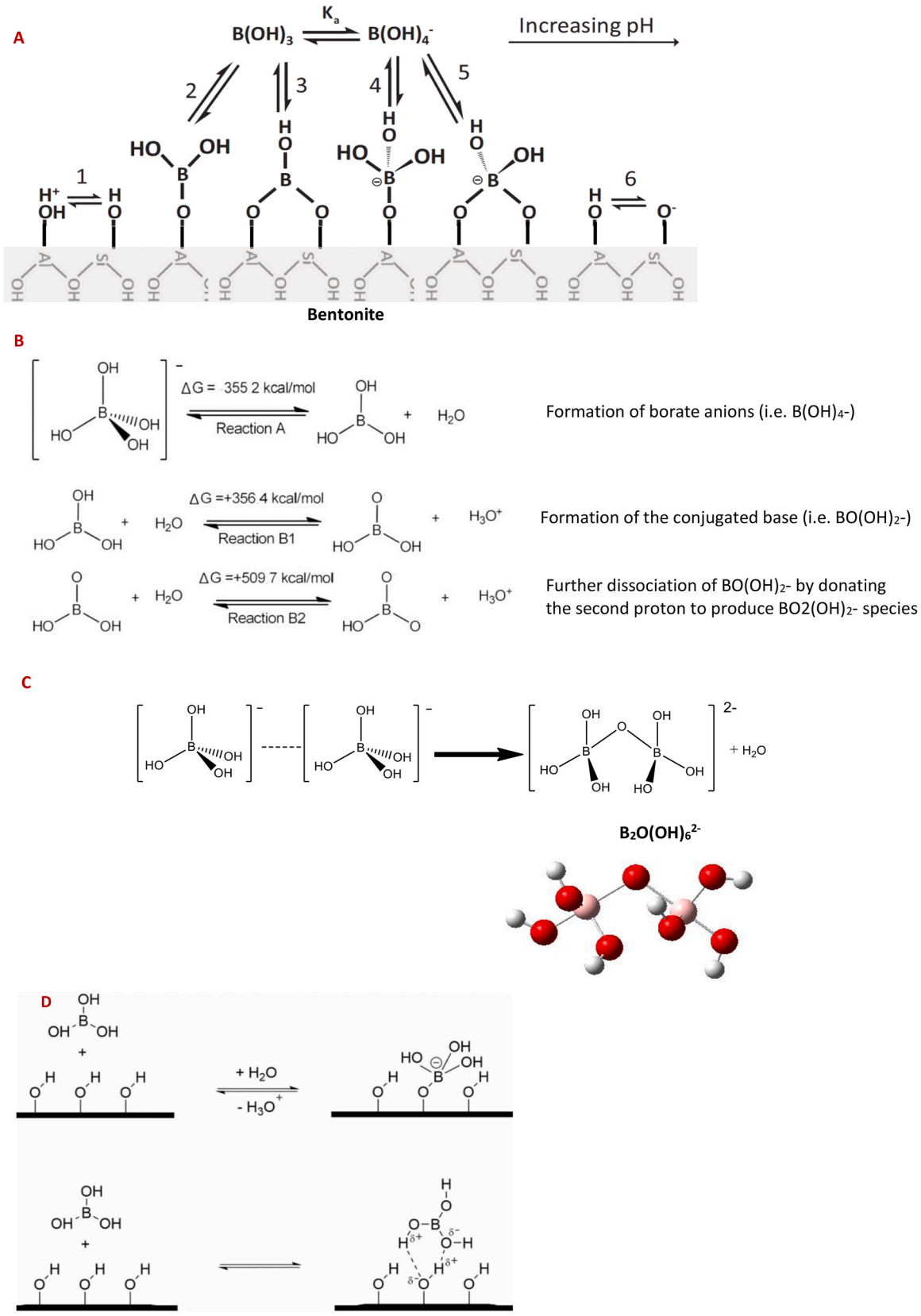

Fig. 10. A. Representative mechanism of boron adsorption on bentonite. Reactions 1 and 6 are surface group deprotonation; reactions 2 and 4 are monodentate complexation; reactions 3 and 5 are bidentate complexation (modified from Lin et al., 2021), **B.** Different pathways of dissociation reaction of boric acid (i.e. H_3BO_3) in aqueous solution at 298 K, **C.** Polymerization of monomeric borate anions species into $B_2O(OH)_6^{2-}$ (Wang et al., 2018), and **D.** Adsorption of boric acid onto RDPs, esterification reaction and hydrogen bonds (Lin et al., 2021).

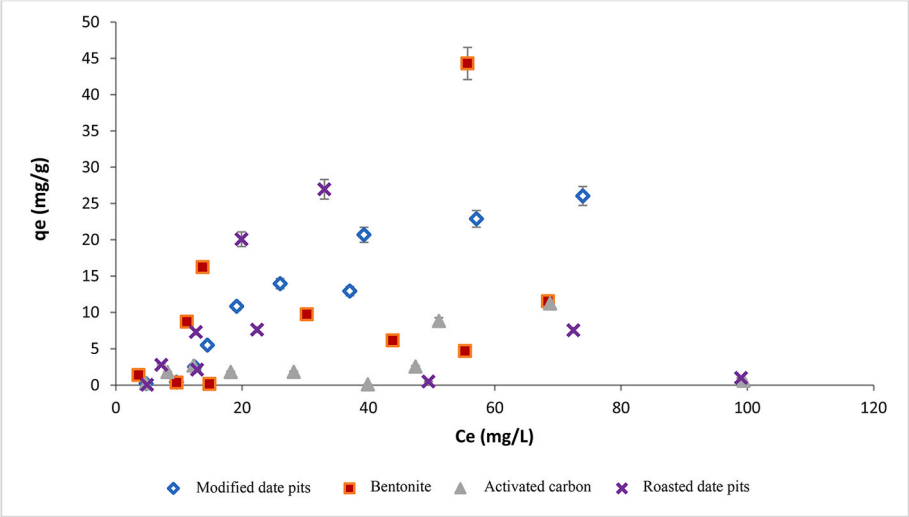

Fig. 11. Study of the impact of concentration on the adsorption process of boron.

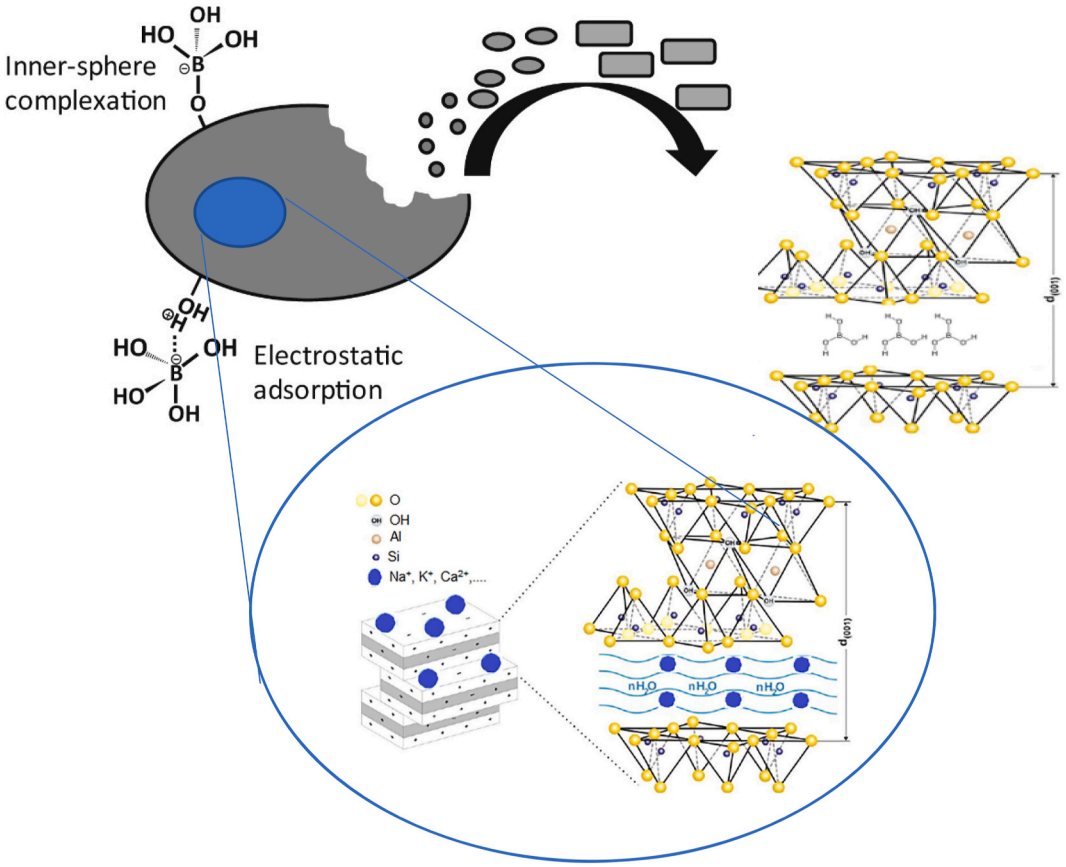

Fig. 12. Adsorption mechanism of boron onto bentonite (Lin et al., 2021; Bananezhad et al., 2019).

Table 3
The effect of temperatures on the adsorption of boron.

Adsorbent	Removal Efficiency %		
	at 25 °C	at 35 °C	at 45 °C
AC	18.00	55.38	91.25
Bentonite	54.16	66.10	59.85
RDPs	44.96	40.13	45.58
MDPs	36.18	56.17	71.69

Furthermore, increasing the boron concentration resulted in enhanced boron diffusion into the inner pores. In addition, it is shown that there is a fluctuating trend of increasing and decreasing the adsorption capacity as a consequence of the active sites' heterogeneity and potential chemical bindings such as surface complexation and/or mono-, di, and tri-coordination of boron. The adsorbent's surface had several different functional groups such as hydroxyl, ether, and carbonyl; hence, considerably influence the adsorption mechanisms. The fluctuation trend of increasing and decreasing bromide ions adsorption by RDPs was

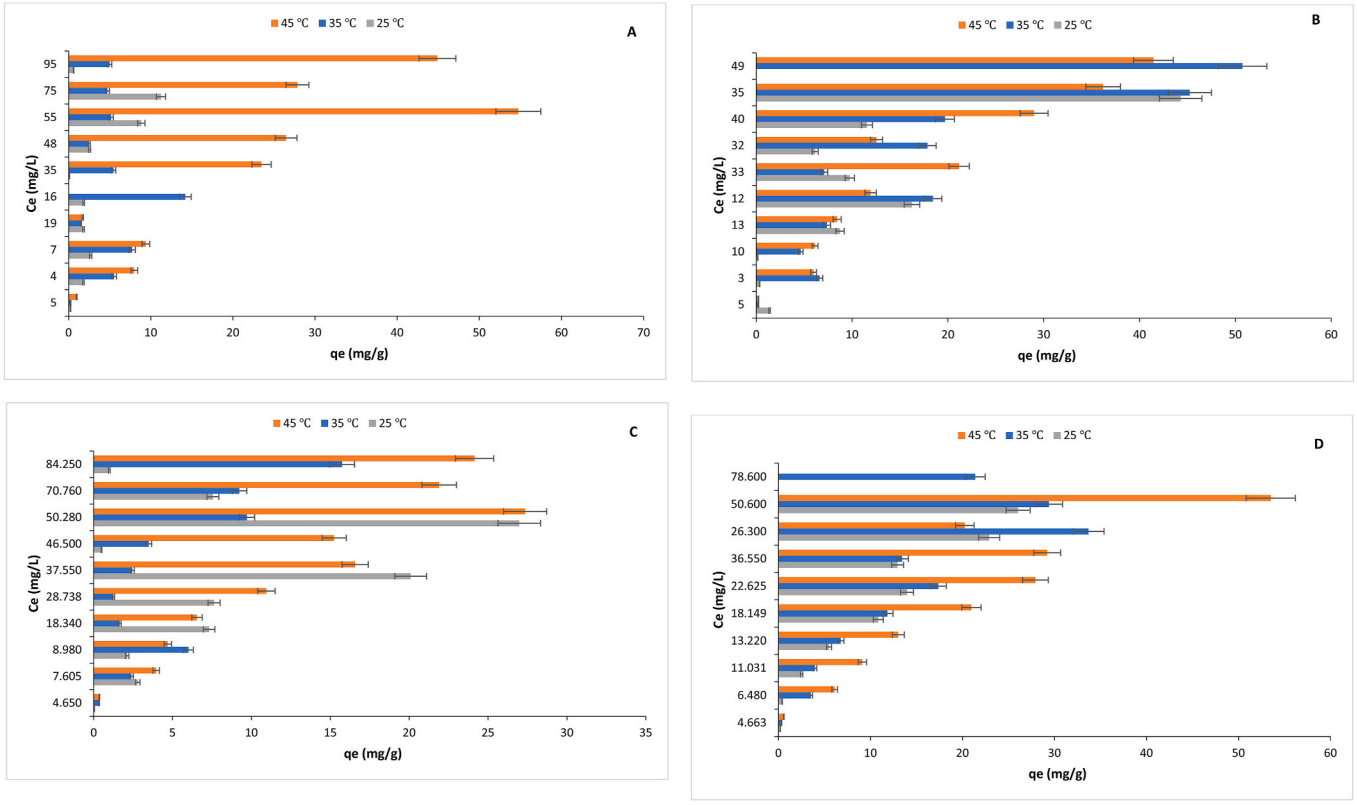

Fig. 13. Study of the influence of temperature on boron adsorption using (A) activated carbon, (B) bentonite, (C) RDPs, and (D) MDPs.

also observed by Al-Ghouti et al. (2017).

3.7. Effect of temperature on boron removal

Table 3 shows the effect of temperature on the adsorption of boron using AC, bentonite, RDPs, and MDPs. Fig. 13 illustrates the influence of temperature values 25, 35 and 45 °*C* on boron adsorption using AC, bentonite, RDPs, and MDPs, respectively. The adsorption efficiency of boron increases at 45 °*C* using AC, RDPs, and MDPs. The maximum adsorption efficiency reached 91% for AC, 72% for MDPs, and 46% for RDPs. While the adsorption efficiency of boron increases at 35 °*C* using bentonite that reached the maximum adsorption efficiency of 66%. The highest adsorption capacity of AC was obtained at 45 °*C* with an adsorption capacity of 54.75 mg/g, 27.35 mg/g for RDP, and 50.75 mg/g for bentonite at 35 °*C*, while MDPs were had adsorption capacity of 53 mg/g at 45 °*C*. The increase in adsorption efficiency with temperature is attributed to the increase in viscosity. However, the removal efficiency decreased at 25 °*C* because of the low boron mobility than at higher temperatures, which could prevent it from adsorption at active adsorption sites. At 25 °*C*, the adsorption efficiency decreased to 18% for AC and 36% using MDPs. While the adsorption efficiency decreases to 40% at 35 °*C* using the RDPs.

3.8. Adsorption isotherm model

Four adsorption models were utilized to explore the adsorption process: Langmuir, Dubinin-Radushkevich, Freundlich, and Temkin, and their parameters are summarized in Table 4. The determination of the R^2 coefficient and chi-square χ^2 is used to find the best-fit model for the experimental data. The coefficient of determination R^2 and X^2 is calculated for each model using equations (7) and (8) respectively.

$$R^2 = 1 - \frac{\sum_{i=1}^{n}(q_{i,\,exp} - q_{i,\,mod})^2}{\sum_{i=1}^{n}(q_{i,\,exp} - q_{i,\,exp,mean})^2} = 1 - \frac{SSE}{SST} \quad (7)$$

$$\chi^2 = \sum_{i=1}^{n}\frac{(q_{i,\,exp} - q_{i,mod})^2}{q_{i,\,mod}} \quad (8)$$

Where $q_{i,\,exp}$ and $q_{i,\,mod}$ are the equilibrium capacity (mg/g) taken from the experimental (observed) and model (predicted) data respectively, n is the number of sample sizes, SST is the sum of the square of total deviation and SSE is the sum of square error (Bonilla-Petriciolet et al., 2019).

The R^2 value is sensitive to outliers, which could mislead in fitting the model. Thus, χ^2 is also utilized to determine the good fit model. Critical Chi (p-value) for n = 10 is 18.31 at $\alpha = 0.05$ and 23.21 at $\alpha = 0.01$, if the χ^2 is lower than the p-value, the null hypothesis is not rejected, and it is concluded that there is no sufficient evidence that the experimental value is different from the model value.

The non-fitted plot of the Langmuir model for boron adsorption using AC and RDPs showed two different linear lines; one line is at low concentrations, and the other is at high concentrations. This indicates the heterogeneous adsorption in which the highest adsorption energy sites are adsorbed first, and then the second adsorption energies are created allowing more adsorption at high concentrations. The creation of the second adsorption site is explained by the high concentration of adsorbate that creates pressure on the adsorbent surface and forces the adsorbates into the internal surface and pores. In addition, it could be explained by the formation of new adsorption sites due to the pressure force that removes blocks that hinder the adsorbates from entering the pores (Al-Ghouti et al., 2010). Temkin isotherm model is the best fit to describe the adsorption of boron by bentonite at 45 °*C* ($R^2 = 0.73$ and $\chi^2 = 19$), the adsorption of boron by MDPs at 35 °*C* ($R^2 = 0.91$ and $\chi^2 = 3.5$), and the adsorption of boron by RDPs at 45 °*C* ($R^2 = 0.83$ and $\chi^2 = 9.3$). Freundlich isotherm model describes well the adsorption of boron by MDPs at 35 °*C* ($R^2 = 0.86$ and $\chi^2 = 42$).

Table 4
Adsorption isotherm models parameters for the adsorption process of boron by AC, bentonite, RDPs, and MDPs.

Model	Temperature	Parameter	AC	Bentonite	RDPs	MDPs
Langmuir	25	Q_o (mg/g)	−34	0.083	−0.38	−1.0
		b (L/mg)	−0.0018	0.027	−0.034	−0.035
		R^2	0.57	0.50	0.56	0.90
		χ^2	34	2200	32	63
	35	Q_o (mg/g)	57	−9.8	−23	−2.2
		b (L/mg)	0.0022	−0.015	−0.0043	−0.038
		R^2	0.28	0.22	0.61	0.67
		χ^2	178	359	36	33
	45	Q_o (mg/g)	6.1	222	−2.8	−6.39
		b (L/mg)	0.38	0.0033	−0.035	−0.046
		R^2	0.038	0.84	0.62	0.29
		χ^2	159	11	376	1.9E05
Freundlich	25	1/n	0.73	0.55	0.66	1.8
		K_f (mg/g) $(L/mg)^{1/n}$	0.16	1.4	1.0	0.017
		R^2	0.19	0.32	0.28	0.86
		χ^2	40	116	51	42
	35	1/n	0.28	1.1	0.80	1.3
		K_f (mg/g) $(L/mg)^{1/n}$	1.48	0.36	0.24	0.17
		R^2	0.084	0.50	0.50	0.72
		χ^2	57	125	30	68
	45	1/n	0.53	1.2	1.2	1.1
		K_f (mg/g) $(L/mg)^{1/n}$	2.3	0.27	0.21	0.92
		R^2	0.13	0.62	0.76	0.54
		χ^2	146	54	31	84
Dubinin-Radushkevich	25	q_s (mg/g)	2.07	11	6.4	25
		K (mol^2/kJ^2)	-9×10^{-06}	-5×10^{-06}	-2×10^{-05}	-7×10^{-05}
		R^2	0.16	0.28	0.46	0.97
		χ^2	67	336	36	45
	35	q_s (mg/g)	4.8	15	5.0	19
		K (mol^2/kJ^2)	-4×10^{-06}	-5×10^{-06}	-1×10^{-05}	-2×10^{-05}
		R^2	0.16	0.27	0.46	0.88
		χ^2	43	185	42	26
	45	q_s (mg/g)	22	19	18	37
		K (mol^2/kJ^2)	-8×10^{-07}	-9×10^{-06}	-1×10^{-05}	-8×10^{-06}
		R^2	0.14	0.49	0.89	0.66
		χ^2	382	91	41	52
Temkin	25	B (J/mol)	1.6	6.1	1.2	10
		b_t	1545	402	2004	234
		At (L/mg)	0.27	0.24	21	0.13
		R^2	0.17	0.20	0.017	0.91
		χ^2	23	83	692	3.5
	35	B (J/mol)	−0.213	12	3.2	9.9
		b_t	−11636	198	764	248
		At (L/mg)	6×10^{-08}	0.24	0.20	0.21
		R^2	0.016	0.46	0.43	0.61
		χ^2	–	22	23	25
	45	B (J/mol)	5.07	12	9.2	16
		b_t	488	191	268	146
		At (L/mg)	4.2	0.22	0.21	0.33
		R^2	0.093	0.73	0.83	0.62
		χ^2	112	19	9.3	15

Table 5
Thermodynamic parameters of boron adsorption.

Adsorbent	Temperature ° *C*	ln b or ln K_f [a]	ΔG° (kJ/mol)	ΔH° (kJ/mol)	ΔS° (J/mol.K)
AC	25	−1.8	−25	150	580
	35	4.0	−30		
	45	1.8	−36		
Bentonite	25	−2.5	5.5	47	140
	35	−1.0	4.1		
	45	−1.3	2.7		
RDPs	25	0	−0.49	−61	−203
	35	−0.2	1.5		
	45	−1.5	3.5		
MDPs	25	−4.0	9.9	160	495
	35	−1.8	4.9		
	45	−0.31	0.015		

[a] Langmuir isotherm constant (b) or Freundlich isotherm constant (K_f) depend on the applicability of the models.

3.9. Thermodynamic study

Table 5 shows the thermodynamic parameters for boron adsorption. To understand the adsorption process, thermodynamic parameters are required. Thermodynamic studies estimate standard Gibbs free energy change (ΔG °), standard enthalpy change (ΔH °), and standard entropy change (ΔS °). These parameters aid in verifying the favorability, spontaneity, endothermicity, or exothermicity of the adsorption process. In addition, it helps to investigate the adsorption nature, such as physical adsorption or chemical adsorption (Al-Ghouti and Da'ana, 2020). Physical adsorption is an exothermic process that is characterized by the heat of adsorption lower than 20 kJ/mol for van der Waals, and it is from 20 kJ/mol to 80 kJ/mol for electrostatic interaction, while it is from 80 kJ/mol to 450 kJ/mol for chemical adsorption (Bonilla-Petriciolet et al., 2017). The estimation of the adsorption thermodynamic parameters is found by plotting (1/T) versus (ln b), where (b) is Langmuir isotherm constant, or ln (K_f), where (K_f) is Freundlich isotherm constant,

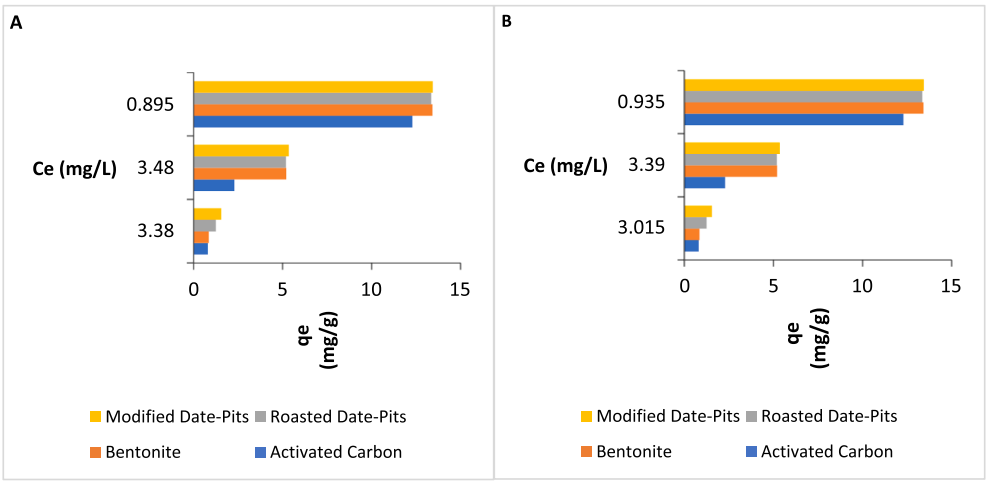

Fig. 14. Boron adsorption from GW samples, **A.** at 25 °C and **B.** 35 °C.

depending on the applicability of the model. The adsorption of boron on AC at 25 °C, 35 °C, and 45 °C showed negative values for free energy that indicated a spontaneous and favorable adsorption process. The value of ΔG° is increased for higher temperatures showing more favorable and spontaneous adsorption at high temperatures. However, the positive value of ΔH° inferred that experiment favored an endothermic pathway, and the magnitude of ΔH° from 150 kJ/mol to 180 kJ/mol can give an idea that electrostatic interaction and chemical adsorption occur between the adsorbent and adsorbate. In relation to the positive entropy values that suggest dissociative adsorption and the possibility of some structural changes or readjustments in the adsorbate–adsorbent that forms an active complex. Finally, (TΔS°) contributes more than ΔH°, thus the adsorption is an entropy-controlled process.

3.10. Real GW adsorption experiments

Three real GW samples were used to study the adsorption of boron using AC, bentonite, RDPs, and MDPs. More details about the characteristics of the used GW and its metal content can be found in our previous publication (Ahmad et al., 2020). The concentrations of boron for the three studied GW samples are "GW Sample 1" 4.523 mg/L, "GW Sample 2" 4.101 mg/L, and "GW Sample 3" 1.502 mg/L. The adsorption experiment has been conducted at pH 7 to compare the result with real water pH (mean value of 7.3). Fig. 14 presents the boron adsorption

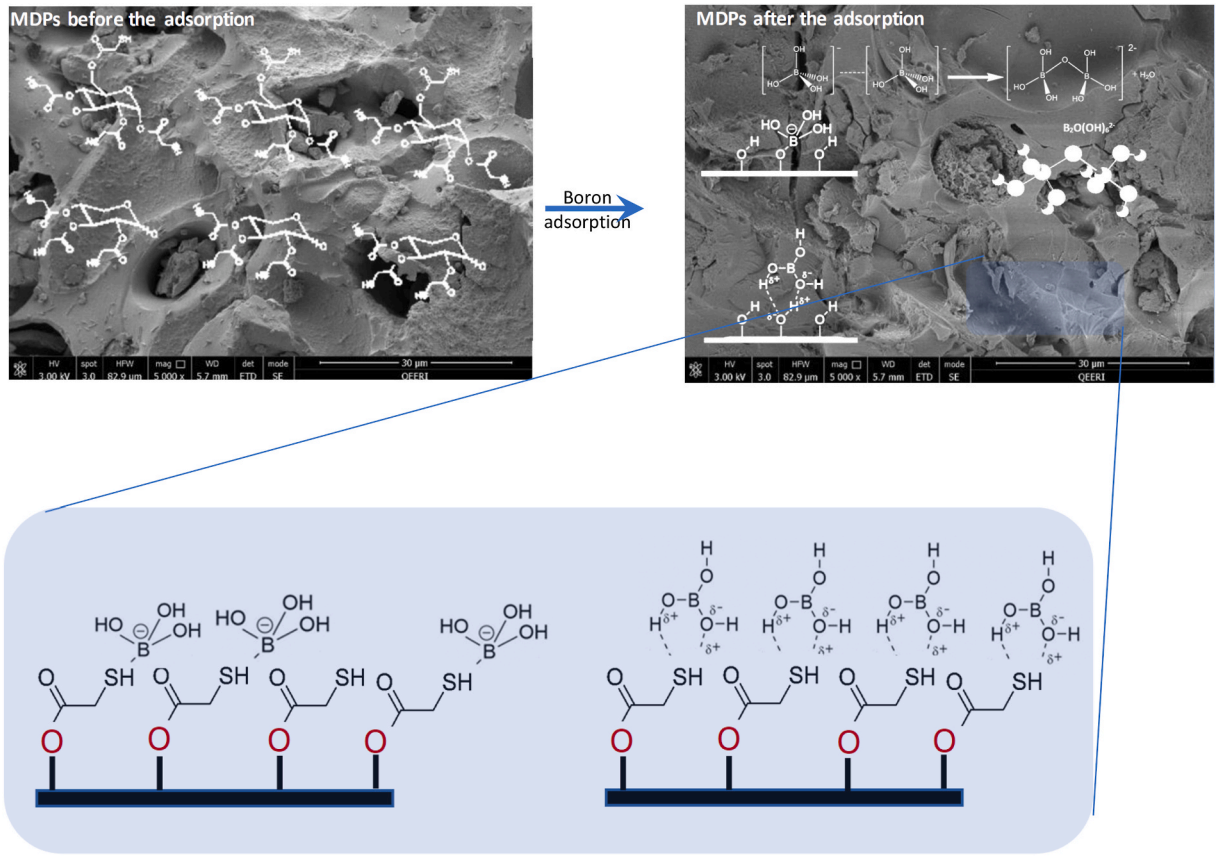

Fig. 15. Schematic diagram of boron adsorption onto MDPs.

capacity from GW samples at 25 °C and 35 °*C*. The adsorption of boron decreased with the increase in boron concentration in the GW samples due to the competition with other pollutants such as molybdenum and lithium available in the GW on the active sites. The highest percent of boron removal is in "GW sample 3" due to the availability of active sites for boron adsorption. The maximum percent of boron removal at 25 °*C* is 44% using RDPs with an adsorption capacity of 13.34 mg/g, followed by bentonite, AC, and MDPs with 42%, 40%, and 39%, respectively. The adsorption capacity obtained by bentonite was 13.4, by AC 12.28, and by MDPs 13.42 mg/g. The adsorption of boron decreases at 35 °*C* in the samples that have low boron concentration, while it increases at 35 °*C* for high concentration samples due to increasing boron ions mobility that bombarded with some adsorbed ions and the hence restructure of the adsorption ions. The maximum percent of boron removal at 35 °*C* is 40% using MDPs followed by RDPs, AC, and bentonite with 38%, 37%, and 36%, respectively. The obtained adsorption capacity was 13.42 mg/g for MDPs, 13.34 mg/g for RDPs, 12.28 mg/g by AC, and 13.4 mg/g for bentonite.

In a slightly alkaline aqueous solution, the dominant species of boron are borate anions $B(OH)_4^-$ as shown by the equilibrium reaction equation (9),

$$H_3BO_3 + H_2O \leftrightarrow B(OH)_4^- + H^+ \quad (9)$$

Date pits consist of about 17.5% hemicellulose, 11.0% lignin, and 42.5% cellulose (Al-Ghouti et al., 2010). Lignin is considered as the cementing matrix that holds cellulose and hemicellulose units together; while cellulose and hemicellulose contain oxygenated functional groups such as hydroxyl, ether, and carbonyl (Hawari et al., 2014). This is supported by the FTIR results that showed the availability of the different oxygenated functional groups such as hydroxyl, carboxyl, and thiol groups that indicate the possibility of chemical adsorption mechanisms besides the physical adsorption. Physical adsorption is supported by the physical analysis results using SEM and BET that showed the high surface area and the pores volume of AC and MDPs adsorbents that enhanced the adsorption capacity. While the availability of the negative active functional groups indicates chemical adsorption mechanisms such as hydrogen bond, electrostatic interaction, and/or complexation. Thus, the proposed adsorption mechanisms onto the MDPs active sites are dispersion forces known as van der Waal's forces, electrostatic interaction, and/or complexation. The $B(OH)_4^-$ anions are repelled with negatively charged functional groups. The proposed mechanisms for $B(OH)_4^-$ adsorption is when cellulose and/or lignin capture free proton during the complexing of borate by functional groups such as hydroxyl which then interact with borate ion through a covalent attachment and form a coordination complex. Fig. 15 illustrates the schematic diagram of boron adsorption onto MDPs.

3.11. Statistical analysis

The ANOVA single factor test was conducted to test the influence of pH on boron adsorption using AC, bentonite, RDPs, and MDPs. There is no significant difference between the absorbates' concentrations and pH value as the $F < F_{Critical}$, and p-value ≥ 0.05, and the null hypothesis of equal means is accepted. The two-factor ANOVA with replication test was conducted to test the relation between temperature and concentration using AC, bentonite, RDPs, and MDPs. Boron concentrations are not significantly different between different temperatures because the p-value ≥ 0.05. In addition, there is a highly significant difference between (column) the adsorbents namely AC, bentonite, RDPs, and MDPs as the $F > F_{Critical}$, and p-value ≤ 0.05.

4. Conclusion

The use of MDPs to remove boron from groundwater was found to be an efficient adsorption approach. Date pits are agricultural waste; thus, it has environmental and economic benefits to use as adsorbents. The pH, initial adsorbate concentration, and temperature were all investigated to optimize the effectiveness of the adsorbent process. It was discovered that pH 6 has a substantial impact on the adsorption process since it changes the interaction of the adsorbate with the adsorbent's surface. Moreover, the adsorption process MDPs was favorable indicating the spontaneity and endothermicity of the process. The adsorption of boron onto MDPs was successful due to the presence of different oxygenated functional groups as confirmed by FTIR analysis. Thus, this work showed that MDPs are valuable for remediating boron from groundwater. It is indicated by the negative values of the free energy that at high temperatures the adsorption process is spontaneous and more favorable. The positive entropy values that controlled the adsorption process show that the adsorbate–adsorbent complex may undergo some structural changes or readjustments.

Declaration of competing interest

The authors declare that they have no known competing financial interests or personal relationships that could have appeared to influence the work reported in this paper.

Acknowledgment

This publication was made possible by NPRP grant # [12S-0307-190250] from the Qatar National Research Fund (a member of Qatar Foundation). The findings achieved herein are solely the responsibility of the author[s]. Thanks to Mrs. Dana Da'na and Mrs. Mariam Khan for their assistance in the analysis of the sample. Open Access funding provided by the Qatar National Library.

References

Ahmad, Tanweer, Mohammad, Danish, Rafatullah, Mohammad, Arinza, Ghazali, Othman, Sulaiman, Rokiah, Hashim, Mohamad, Ibrahim, 2011. The use of date palm as a potential adsorbent for wastewater treatment: a review. Environ. Sci. Pollut. Control Ser. 19 (5), 1464–1484. https://doi.org/10.1007/s11356-011-0709-8.

Ahmad, Ayesha, Al-Ghouti, Mohammad, Majeda, Khraisheh, Nabil, Zouari, 2020. Hydrogeochemical characterization and quality evaluation of groundwater suitability for domestic and agricultural uses in the state of Qatar. Groundwater For Sustainable Development 11, 100467. https://doi.org/10.1016/j.gsd.2020.100467.

Al-Ghouti, Mohammad, Da'ana, Dana, 2020. Guidelines for the use and interpretation of adsorption isotherm models: a review. J. Hazard Mater. 393, 122383. https://doi.org/10.1016/j.jhazmat.2020.122383.

Al-Ghouti, Mohammad, Khan, Mariam, 2018. Eggshell membrane as a novel bio sorbent for remediation of boron from desalinated water. J. Environ. Manag. 207, 405–416. https://doi.org/10.1016/j.jenvman.2017.11.062.

Al-Ghouti, Mohammad, Li, Juiki, Salamh, Yousef, Al-Laqtah, Nasir, Walker, Gavin, Ahmad, Mohammad, 2010. Adsorption mechanisms of removing heavy metals and dyes from aqueous solution using date pits solid adsorbent. J. Hazard Mater. 176 (1–3), 510–520. https://doi.org/10.1016/j.jhazmat.2009.11.059.

Al-Ghouti, Mohammad, Al-Disi, Zulfa, Nasser, Alkaabi, Majeda, Khraisheh, 2017. Mechanistic insights into the remediation of bromide ions from desalinated water using roasted date pits. Chem. Eng. J. https://doi.org/10.1016/j.cej.2016.09.091.

Al-Ghouti, Mohammad, Dana, Da'ana, Abu-Dieyeh, Mohammed, Majeda, Khraisheh, 2019. Adsorptive removal of mercury from water by adsorbents derived from date pits. Sci. Rep. 9 (1) https://doi.org/10.1038/s41598-019-51594-y.

Al-Haddabi, Mansour, Ahmed, Mushtaque, Al-Jebri, Zainab, Hari, Vuthaluru, Hussein, Znad, Al-Kindi, Mohammed, 2015. Boron removal from seawater using date palm (*Phoenix dactylifera*) seed ash. Desalination Water Treat. https://doi.org/10.1080/19443994.2014.1000385.

Alhamed, Yahia, 2009. Adsorption kinetics and performance of packed bed adsorber for phenol removal using activated carbon from dates' stones. J. Hazard Mater. 170, 763–770, 2009.

Al-Ithari, Al-Ithari, Arumugam, Sathasivan, Ahmed, Roxanne, Hari, Vuthaluru, Zhan, Weixi, Ahmed, Mushtaque, 2011. Superiority of date pits ash as an adsorbent over other ashes and ferric chloride in removing boron from seawater. Water Treat. 32, 324–328, 2011.

Al-Jlil Saad, 2015. Characterization and application of bentonite clay for lead ion adsorption from wastewater: equilibrium and kinetic study. Res. J. Environ. Sci. 9 (1), 1–15. https://doi.org/10.3923/rjes.2015.1.15.

Akpomie, Kovo, Dawodu, Folasegun, 2015. Potential of a low-cost bentonite for heavy metal abstraction from binary component system. Beni-Suef University Journal of Basic and Applied Sciences 4 (1), 1–13. https://doi.org/10.1016/j.bjbas.2015.02.002.

Andrade, Bastos, Gianesi, Toffoli, Valenzuela-Díaz, 2018. Adsorption and Surface Area of Modified Bentonite Used as Bleaching Clay. https://doi.org/10.1007/978-3-319-72484-3_36.

Bananezhad, Behjat, Islami, Mohammad, Ghonchepour, Ehsan, Mostafavi, Hamid, Tikdari, Ahmad, Rafiei, Hamid, 2019. Bentonite clay as an efficient substrate for the synthesis of the super stable and recoverable magnetic nanocomposite of palladium (Fe3O4/Bentonite-Pd). Polyhedron 162, 192–200. https://doi.org/10.1016/j.poly.2019.01.054.

Bhagyaraj, Sneha, Mohammad, Al-Ghouti, Kasak, Peter, Igor, Krupa, 2021. An updated review on boron removal from water through adsorption processes. Emergent Materials 4 (5), 1167–1186. https://doi.org/10.1007/s42247-021-00197-3.

Bodzek, Micha, 2015. The removal of boron from the aquatic environment–state of the art. Desalination Water Treat. 57 (3), 1107–1131. https://doi.org/10.1080/19443994.2014.1002281.

Bonilla-Petriciolet, Adrian, Mendoza-Castillo, Didilia, Guilherme, Dotto, Carlos, Duran-Valle, 2019. Adsorption in water treatment. Reference Module in Chemistry, Molecular Sciences and Chemical Engineering. https://doi.org/10.1016/b978-0-12-409547-2.14390-2.

Bonilla-Petriciolet, Adrian, Mendoza-Castillo, Didilia, Reynel-Ávila, Hilda, 2017. Introduction. Adsorption Processes for Water Treatment and Purification 1–18. https://doi.org/10.1007/978-3-319-58136-1_1.

Corti, Horacio, Crovetto, Rosa, 1980. Properties of the borate ion in dilute aqueous solutions. J. Chem. Soc. Faraday Trans. 1: Phys. Chem. Condens. Phases 76, 2179. https://doi.org/10.1039/f19807602179.

Crini, Gregorio, Lichtfouse, Eric, Wilson, Lee, Nadia, Morin-Crini, 2018. Conventional and non-conventional adsorbents for wastewater treatment. Environ. Chem. Lett. 17 (1), 195–213. https://doi.org/10.1007/s10311-018-0786-8.

Djilani, Chahrazed, Zaghdoudi, Rachida, Djazi, Faycal, Bouchekima, Bachir, Lallam, Abdelaziz, Modarressi, Ali, Rogalski, Marek, 2015. Adsorption of dyes on activated carbon prepared from apricot stones and commercial activated carbon. J. Taiwan Inst. Chem. Eng. 53, 112–121. https://doi.org/10.1016/j.jtice.2015.02.025. ISSN 1876-1070.

Dodbiba, Gjergj, Ponou, Josiane, Toyohisa, Fujita, 2015. Biosorption of heavy metals. Microbiology for Minerals, Metals, Materials and the Environment 427–444. https://doi.org/10.1201/b18124-20.

El-Hendawy Abdel-Nasser, 2006. Variation in the FTIR spectra of a biomass under impregnation, carbonization and oxidation conditions. J. Anal. Appl. Pyrol. 75 (2), 159–166. https://doi.org/10.1016/j.jaap.2005.05.004.

Elsaid, Khaled, 2017. Development, Modeling, Analysis, and Optimization of a Novel Inland Desalination with Zero Liquid Discharge for Brackish Groundwaters. UWSpace. PhD Dissertation, University of Waterloo, Ontario, Canada, p. 173.

Esmeray, Ertugrul, Aydin, Mehmet, 2008. Comparison of natural radioactivity removal methods for drinking water supplies: a review. J. Int. Environ. Appl. Sci. 3, 142–146.

Guan, Zhimin, Lv, Jiafei, Peng, Bai, Guo, Xianghai, 2016. Boron removal from aqueous solutions by adsorption — a review. Desalination 383, 29–37. https://doi.org/10.1016/j.desal.2015.12.026.

Harris, Daniel, 2011. Quantitative Chemical Analysis, eighth ed. Freeman and Company. 13: 978-1429263092, 2011.

Hasenmueller, E.A., Criss, R.E., 2013. Multiple sources of boron in urban surface waters and groundwaters. Sci. Total Environ. 447, 235–247. https://doi.org/10.1016/j.scitotenv.2013.01.001.

Hawari, Alaa, Khraisheh, Majeda, Al-Ghouti, Mohammad, 2014. Characteristics of olive mill solid residue and its application in remediation of pb2+, cu2+ and ni2+ from aqueous solution: mechanistic study. Chem. Eng. J. 251, 329–336. https://doi.org/10.1016/j.cej.2014.04.065.

Horsfall, Michael, Ayebaemi, Spiff, Augustine, Abia, 2004. Studies on the influence of mercaptoacetic acid (MAA) modification of cassava (manihotsculenta cranz) waste biomass on the adsorption of Cu^{2+} and Cd^{2+} from aqueous solution. Bull. Kor. Chem. Soc. 25 (7), 969–976.

Huang, Fengyu, Yi, Facheng, Wang, Zhe, Li, Haifeng, 2016. Sorptive removal of Ce(IV) from aqueous solution by Bentonite. Procedia Environmental Sciences 31, 408–417. https://doi.org/10.1016/j.proenv.2016.02.073.

Jiang, J.-Q., Xu, Y., Quill, K., Simon, J., Shettle, K., 2014. Mechanisms of boron removal with electrocoagulation. Environ. Chem. 3 (5), 350–354. https://doi.org/10.1071/EN06035.

Karahan, Senem, Muruvvet, Yurdakoç, Yoldas, Seki, Yurdakoç, Kadir, 2006. Removal of boron from aqueous solution by clays and modified clays. J. Colloid Interface Sci. 293 (1), 36–42. https://doi.org/10.1016/j.jcis.2005.06.048.

Köse, Ennil, Demiral, Hakan, Öztürk, Nese, 2011. Adsorption of boron from aqueous solutions using activated carbon prepared from olive bagasse. Desalination Water Treat. 29 (1–3), 110–118. https://doi.org/10.5004/dwt.2011.2091.

Lin, Jui, Nicolaus, Mahasti, Yao-Hui, Huang, 2021. Recent advances in adsorption and coagulation for boron removal from wastewater: a comprehensive review. J. Hazard Mater. 407, 124401. https://doi.org/10.1016/j.jhazmat.2020.124401.

Liu, Zhi, Shao, Ming, Wang, Yun, 2012. Large-scale spatial interpolation of soil pH across the Loess Plateau, China. Environ. Earth Sci. 69 (8), 2731–2741. https://doi.org/10.1007/s12665-012-2095-z.

Lopalco, Antonio, Lopedota, Angela, Laquintana, Valentino, Denora, Nunzio, Stella, Valentino, 2020. Boric acid, a lewis acid with unique and unusual properties: formulation implications. J. Pharmaceut. Sci. 109 (8), 2375–2386. https://doi.org/10.1016/j.xphs.2020.04.015.

Masindi, Vhahangwele, Gitari, Mugera, Tutu, Hlanganani, Debeer, Marinda, 2015. Removal of boron from aqueous solution using magnesite and bentonite clay composite. Desalination Water Treat. https://doi.org/10.1080/19443994.2015.1025849.

MDPS, Ministry of Development Planning and Statistics, 2017. Water Statistics in the State of Qatar 2018. Retrieved March 1, 2020, from. https://www.psa.gov.qa/ar/statistics1.

MDPS, Ministry of Development Planning and Statistics, 2018. Population Statistics in the State of Qatar 2018. Retrieved March 1, 2020, from. https://www.psa.gov.qa/ar/statistics1.

Miessler, Gray, Fischer, Paul, Tarr, Donald, 2014. Inorganic Chemistry. Pearson, Harlow, Essex, 13: 978-0321811059.

Minceva, Mirjana, Markovska, Fajgar, Meshko, Verka, 2008. Comparative study of Zn2+, Cd2+, and Pb2+removal from water solution using natural clinoptilolitic zeolite and commercial granulated activated carbon. equilibrium of adsorption. Separ. Sci. Technol. 43 (8), 2117–2143. https://doi.org/10.1080/01496390801941174.

Nagul, Edward, Mckelvie, Ian, Worsfold, Paul, Kolev, Spas, 2015. The molybdenum blue reaction for the determination of orthophosphate revisited: opening the black box. Anal. Chim. Acta 890, 60–82. https://doi.org/10.1016/j.aca.2015.07.030.

Ogheneochuko, Oputu, Olushola, Ayanda, Olalekan, Fatoki, Cecilia, Akintayo, Olumayede, Gbenga, Olusola, Amodu, 2017. Water Treatment Technologies: Principles, Applications, Successes and Limitations of Bioremediation, Membrane Bioreactor and the Advanced Oxidation Processes. https://doi.org/10.4172/978-1-63278-058-4-059.

Oyola-Rivera, Oscar, González-Rosario, Alexa, Cardona-Martínez, Nelson, 2018. Catalytic production of sugars and lignin from agricultural residues using dilute sulfuric acid in γ-valerolactone. Biomass Bioenergy 119, 284–292. https://doi.org/10.1016/j.biombioe.2018.09.031.

Pan, Duo-qiang, Fan, Qiao-hui, Li, Ping, Sheng-ping, Liu, Wang-suo, Wu, 2011. Sorption of Th (IV) on Na-bentonite: effects of pH, ionic strength, humic substances and temperature. Chem. Eng. J. 172 (2–3), 898–905. https://doi.org/10.1016/j.cej.2011.06.080.

Peters, J.A., 2014. Interactions between boric acid derivatives and saccharides in aqueous media: structures and stabilities of resulting esters. Coord. Chem. Rev. 268, 1–22.

Shafiq, M., Alazba, A.A., Amin, M.T., 2019. Synthesis, characterization, and application of date palm leaf waste-derived biochar to remove cadmium and hazardous cationic dyes from synthetic wastewater. Arabian J. Geosci. 12 (2) https://doi.org/10.1007/s12517-018-4186-y.

Shannon, 1976. Revised effective ionic radii and systematic studies of interatomic distances in halides and chalcogenides. Acta Crystallogr. A 32 (5), 751–767. https://doi.org/10.1107/s0567739476001551.

Smith, Ewen, Dent, Geoffrey, 2019. Modern Raman Spectroscopy a Practical Approach. John Wiley & Sons Inc, pp. 2000–2021, 256.

Socrates, 2015. Infrared and Raman Characteristic Group Frequencies: Tables and Charts, third ed. George Socrates (the University of West, London, Middlesex, U.k. J. Wiley and SONS: Chichester. 2001. ISBN: 0-471-85298-8. (2002). Journal of the American Chemical Society, 124(8), 1830-1830. doi:10.1021/ja0153520.

Strawn, Daniel, 2021. Sorption mechanisms of chemicals in soils. Soil Systems 5 (1), 13. https://doi.org/10.3390/soilsystems5010013.

Wang, Yifeng, Ira, Weinstock, 2012. Polyoxometalate-decorated nanoparticles. Chem. Soc. Rev. 41 (22), 7479. https://doi.org/10.1039/c2cs35126a.

Temesgen, Tatek, Bui, Thi Thuy, Han, Mooyoung, Kim, Tschung-il, Park, Hyunju, 2017. Micro and nanobubble technologies as a new horizon for Water-treatment techniques: a review. Adv. Colloid Interface Sci. 246, 40–51. https://doi.org/10.1016/j.cis.2017.06.011.

Velo-Gala, Inmaculada, López-Peñalver, Jesus, Sánchez-Polo, Manuel, Rivera-Utrilla, Jose, 2014. Surface modifications of activated carbon by gamma irradiation. Carbon 67, 236–249. https://doi.org/10.1016/j.carbon.2013.09.087.

Vilardi, Giorgio, Palma, Luca, Verdone, Nicola, 2018. Heavy metals adsorption by banana peels micro-powder: equilibrium modeling by non-linear models. Chin. J. Chem. Eng. 26 (3), 455–464. https://doi.org/10.1016/j.cjche.2017.06.026.

Wang, Yi-jing, Hai-Zhen, Wei, Jiang, Shao-Yong, van de Ven, Theo, Bao-Ping, Ling, Yin-Chuan, Li, Yi-Bo, Lin, Guo, Qi, 2018. Mechanism of boron incorporation into calcites and associated isotope fractionation in a steady-state carbonate-seawater system. Appl. Geochem. 98, 221–236. https://doi.org/10.1016/j.apgeochem.2018.09.013.

Wulfsberg, 1995. Principles of Descriptive Inorganic Chemistry. University Science Books, Sausalito, 13: 978-0935702668.

Xie, Yanhua, Ren, Lulu, Zhu, Xueqian, Gou, Xi, Chen, Siyu, 2018. Physical and chemical treatments for removal of perchlorate from water–a review. Process Saf. Environ. Protect. 116, 180–198. https://doi.org/10.1016/j.psep.2018.02.009.

Yadav, Sunil Kumar, Singh, Dhruv Kumar, Sinha, Shishir, 2013. Adsorption study of lead (ii) onto xanthated date palm trunk: kinetics, isotherm and mechanism. Desalination Water Treat. 51 (34–36), 6798–6807. https://doi.org/10.1080/19443994.2013.792142.

Yizhak, 1989. Ionic radii in aqueous solutions. ChemInform 20 (17). https://doi.org/10.1002/chin.198917352.

Zhao, 2008. Adsorption of thorium (IV) on MX-80 bentonite: effect of pH, ionic strength and temperature. Appl. Clay Sci. 41 (1–2), 17–23. https://doi.org/10.1016/j.clay.2007.09.012.